Simultaneous Measurement of Bacterial Flagellar Rotation Rate and Swimming Speed

Yukio Magariyama,* Shigeru Sugiyama,* Kazumasa Muramoto,‡ Ikuro Kawagishi,‡ Yasuo Imae,†‡ and Seishi Kudo‡§

*Tsukuba Research Laboratory, Yaskawa Electric Corporation, 5-9-10 Tokodai, Tsukuba 300-26, Japan; ‡Department of Molecular Biology, Faculty of Science, Nagoya University, Chikusa-ku, Nagoya 464-01, Japan; and §PRESTO, JRDC, 5-9-10 Tokodai, Tsukuba 300-26, Japan

ABSTRACT Swimming speeds and flagellar rotation rates of individual free-swimming *Vibrio alginolyticus* cells were measured simultaneously by laser dark-field microscopy at 25, 30, and 35°C. A roughly linear relation between swimming speed and flagellar rotation rate was observed. The ratio of swimming speed to flagellar rotation rate was 0.113 μm, which indicated that a cell progressed by 7% of pitch of flagellar helix during one flagellar rotation. At each temperature, however, swimming speed had a tendency to saturate at high flagellar rotation rate. That is, the cell with a faster-rotating flagellum did not always swim faster. To analyze the bacterial motion, we proposed a model in which the torque characteristics of the flagellar motor were considered. The model could be analytically solved, and it qualitatively explained the experimental results. The discrepancy between the experimental and the calculated ratios of swimming speed to flagellar rotation rate was about 20%. The apparent saturation in swimming speed was considered to be caused by shorter flagella that rotated faster but produced less propelling force.

INTRODUCTION

Many bacteria swim by rotating their helical flagellar filaments, which act as screw propellers. Flagellar rotation is driven by a flagellar motor embedded in the cell membrane (see a review by Macnab, 1987). The energy source for the flagellar motor is the electrochemical potential gradient of a specific ion (H^+ or Na^+) across the cell membrane (Manson et al., 1977; Matsuura et al., 1977; Hirota and Imae, 1983). Evidence has been accumulated suggesting that FliG, FliM, and FliN together with MotA and MotB are directly involved in the torque-generating process in H^+-driven flagellar motors of *Escherichia coli* and *Salmonella typhimurium* (Yamaguchi et al., 1986; Blair and Berg, 1990; Francis et al., 1994; Oosawa et al., 1994). However, the way that molecular mechanisms convert electrochemical energy into mechanical work has not yet been clarified.

In order to elucidate the energy-conversion mechanism of flagellar motors, several models have been proposed (for example, Berg and Khan, 1982; Oosawa and Hayashi, 1983; Läuger, 1988; also see a review by Schuster and Khan, 1994). In these models, many types of torque-generation mechanisms and interactions between coupling ion and motor components were assumed. At present, however, experimental data of the motor functions to evaluate the proposed models do not seem to be sufficiently obtained.

One of the ways to investigate the mechanism is to analyze the torque characteristics of the flagellar motor. The torque of the rotating motor can be obtained only from the rotation rate by a calculation based on some hydrodynamic assumptions (Lowe et al., 1987; Iwazawa et al., 1993).

The rotation rate of the flagellar motor was first measured with a cell whose flagellum was tethered to a glass surface (Silverman and Simon, 1974). The average flagellar rotation rate of a number of swimming cells was obtained by analysis of vibration of the cell body (Lowe et al., 1987). The rotation rate of a single flagellum on the cell stuck to a glass slide was measured by laser dark-field microscopy (LDM) (Kudo et al., 1990). The rotation rate of free-rotating flagella was much higher than the rotation rate of tethered cells.

Although hydrodynamic models to analyze bacterial motion have been proposed (Holwill and Burge, 1963; Chwang and Wu, 1971; Azuma, 1992; Ramia et al. 1993), the applicability of the models has not been fully evaluated because of difficulties in measuring the fast rotation of flagellar filaments of individual swimming cells. The relation between swimming speeds and flagellar rotation rates was measured for *S. typhimurium* cells under high viscosity conditions by cinematography only in the range of slow rotation below 20 rps (Shimada et al., 1976). The cell had multiple flagella that form a bundle during swimming, which caused difficulties in the analysis.

For other microscopic organisms such as spermatozoa, *Chlamydomonas*, and *Paramecium*, applicability and limitation of hydrodynamic models have been experimentally evaluated (see a review by Gibbons, 1981). Their large dimension (40–100 μm) and slower beating motion of flagella and cilia (30–40 Hz) enabled the analysis by cinematography. For example, not only beating frequency but also flagellar wave form was precisely analyzed for spermatozoa of sea urchin, and the swimming speed that was

Received for publication 30 May 1995 and in final form 7 August 1995.

Address reprint requests to Dr. Seishi Kudo, Tsukuba Research Lab, Yaskawa Electric Company, 5-9-10 Tokodai, Tsukuba 300-26, Japan. Tel.: 81-298-47-0751; Fax: 81-298-47-0765; E-mail: kudo@yaskawa.co.jp.

† Deceased.

0006-3495/95/11/2154/00 $2.00

computed was in good agreement with the speed that was actually measured.

In the present study, by using LDM we measured a wide range of swimming speeds and flagellar rotation rates of individual *V. alginolyticus* cells that have single polar flagella. To explain the experimental results, we proposed a new model.

MATERIALS AND METHODS

Cell growth and preparation

A *V. alginolyticus* mutant, YM42 (smooth swimming, no lateral flagella; Y. Maekawa, I. Kawagishi, Y. Imae, and M. Homma, unpublished data), was used. Cells were grown in HI broth (2.5% heart infusion broth, Difco Laboratories, Inc., Detroit, MI; 1.5% NaCl) with shaking at 37°C. The cells were harvested by centrifugation at late logarithmic phase and suspended in HG medium (50 mM HEPES-KOH, pH 7.0; 5 mM glucose; 5 mM $MgCl_2$) supplemented with 300 mM NaCl. The cell density was adjusted to 10^8/ml. The cells were incubated at 25°C for 1 h before use.

Measurement of flagellar rotation rate and swimming speed

Flagellar rotation rates and swimming speeds of individual cells were simultaneously measured by LDM at 25, 30, or 35°C. A drop of cell suspension was put on a glass slide and covered with a coverslip. The edges of the coverslip were sealed with silicone oil to prevent medium flow. Glass slides and coverslips previously kept at 25, 30, and 35°C were used for the experiments at respective temperatures. Flagellar rotation rate was determined from the light-intensity changes obtained by LDM (Kudo et al., 1990; see also Experimental Results section). The swimming speed of the cell was determined according to Hirota et al. (1983) from the video image recorded at the same time. Data acquisition for each specimen was completed within 2 min to avoid the effects of cell damages. The measurements were performed within 2 h after harvesting the cells.

Measurement of parameters of cell and flagellum

A small amount of the cell suspension was sampled immediately before and after LDM measurement. The samples were negatively stained with 1% phosphotungstic acid (pH 7.4) and observed by transmission electron microscopy (TEM; JEM 1200EXII, JEOL Ltd., Tokyo, Japan). Cell lengths, cell radii, lengths of flagellar filaments, diameters of flagellar filaments, pitches of flagellar helices, and filament lengths per pitch were measured on TEM photographs. The radius of flagellar helix, r, was estimated as follows:

$$r = \frac{\sqrt{l^2 - p^2}}{2\pi} \quad (1)$$

where p is pitch of flagellar helix and l is filament length per pitch.

EXPERIMENTAL RESULTS

Simultaneous measurement of flagellar rotation rate and swimming speed

To measure flagellar rotation rate and swimming speed, LDM was applied to single free-swimming cells. The principle of LDM measurement is shown in Fig. 1. When a cell swims across the focused laser beam, the image of flagellar filament appears as a series of bright spots, since the parts

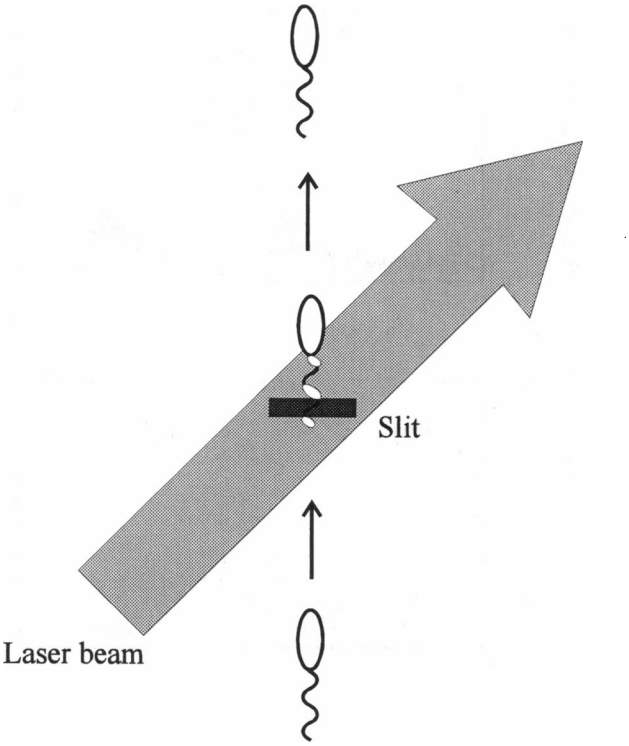

FIGURE 1 Principle of LDM measurement. An image of a bacterium passing over the slit creates a signal that corresponds to the cell body and then the flagellum. The image of helical flagellum illuminated from one side by laser light appears as a series of bright spots. The light-intensity change is detected through the slit and gives information of cell passage and flagellar rotation.

of filament illuminated approximately normally are bright and those illuminated obliquely are dark. As the flagellum rotates, the bright spots move backward while the cell swims forward. The image is focused on an optical slit, and the intensity of light passing through the slit is detected and recorded with a photon counting system. At the same time, the image of the swimming cell is recorded with a video system.

In actual experiments, the light intensity and the video image were continuously recorded for several tens of seconds. The images of some cells passed over the slit during a measurement, and the parts of the records corresponding to the cell passage were selected. It should be noted that if the swimming direction of a cell is within ~5° from the normal of the laser beam, two bright spots per pitch of flagellar helix appear, which gives a twice higher rotation rate. Therefore, we used only the data for the cells whose swimming directions were within 30° from the normal of the slit (within 15–75° from the normal of the laser beam).

Fig. 2 shows an example of light-intensity change obtained by LDM for a cell of *V. alginolyticus*. When an image of a cell body passed across the slit, a large increase in light intensity shown as a "CELL" period in Fig. 2 *a* was observed. The CELL period was followed by an "FLA" period with a smaller increase in intensity,

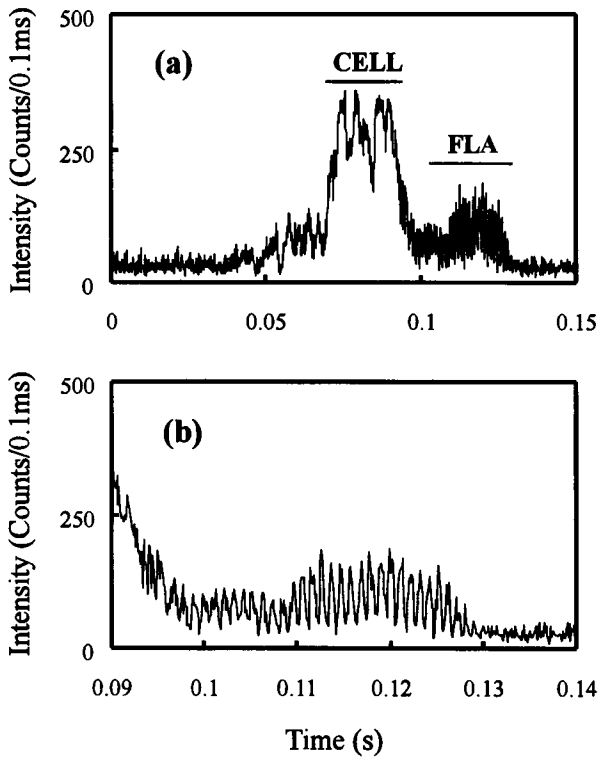

FIGURE 2 An example of light-intensity change obtained for *Vibrio alginolyticus* YM42 by LDM. (*a*) "CELL" and "FLA" indicate the periods when the images of cell and flagellum passed over the slit, respectively. (*b*) "FLA" period in (*a*) is shown with an expanded time scale.

which corresponded to the passage of flagellum. The FLA period is shown with an expanded time scale in Fig. 2 *b*. Rapid and periodic changes in light intensity are clearly seen. One cycle of intensity change corresponds to one flagellar rotation, and the apparent rotation rate, f_{app}, was determined from the average peak interval.

The f_{app} obtained as noted above includes the effect of cell movement. To compensate for the effect, the true rotation rate, f, was determined as follows:

$$f = f_{app} + \frac{v}{p} \quad (2)$$

where v is swimming speed and p is pitch of flagellar helix.

The swimming speed of the same cell was determined from the swimming track recorded with a video system.

It is noteworthy that the light intensity at the beginning of the FLA part was observed to be smaller in most data as in Fig. 2. We also observed with the dark-field microscope that the flagellar images of most swimming bacteria were darker at the proximal ends than the other parts. This part of the flagellum is considered to deviate from the focal plane, which suggests that the bending of the flagellar helix occurs around the proximal end during swimming.

Relation between flagellar rotation rate and swimming speed

Fig. 3 *a* shows the flagellar rotation rate, f, and the swimming speed, v, for individual cells measured by LDM at 25, 30, and 35°C. Both f and v tended to increase with increasing temperature, and a roughly linear relation between f and v was observed. The data points were widely distributed along the solid line in Fig. 3 *a*, which represents the average ratio of v to f of all the data. The deviation of the data from the line was much larger than the errors in determining f and v (3% and 4%).

A ratio of v to f (v-f ratio) indicates how long a cell progresses during one flagellar rotation. The average v-f ratio for all the data was 0.113 μm (Table 1), or 7% of pitch of flagellar helix (1.58 μm, Table 2). There was almost no difference among the average v-f ratios for the data at different temperatures (Table 1), although the torque generated by the flagellar motor and the viscosity of medium are considered to change with temperature. This suggests that the v-f ratio is independent of the motor torque and the viscosity, and dependent on the other parameters that do not change with temperature.

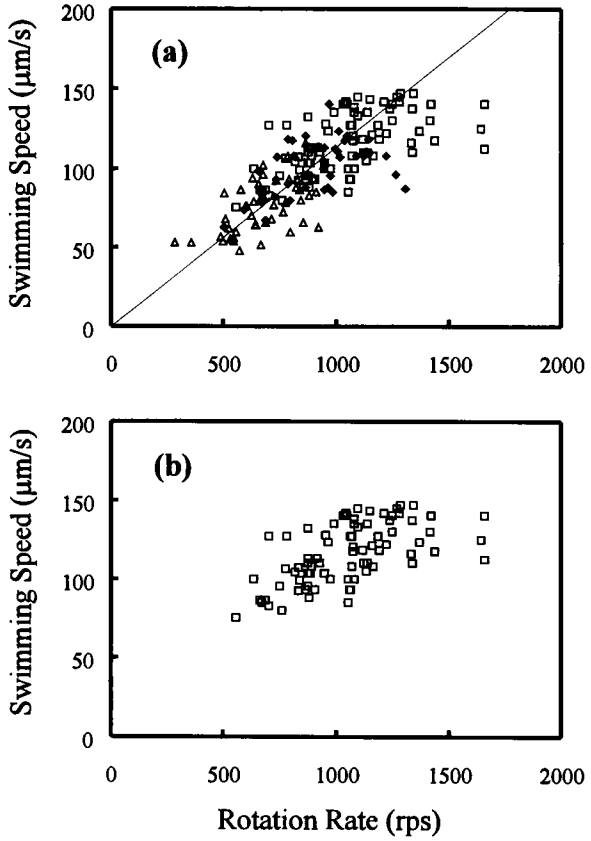

FIGURE 3 Relation between flagellar rotation rate and swimming speed obtained for *V. alginolyticus* YM42. Each point represents data for an individual cell. (*a*) All the data at three different temperatures are shown (*triangle*, 25°C; *diamond*, 30°C; *square*, 35°C). The solid line indicates the average ratio of swimming speed to rotation rate. (*b*) Data obtained at 35°C are replotted.

TABLE 1 Experimental and calculated *v-f* ratios

Temperature (°C)	Average (μm)	SD (μm)	Maximum (μm)	Minimum (μm)	Number of samples
All	0.113	0.021	0.186	0.067	167
25	0.114	0.024	0.186	0.068	47
30	0.112	0.019	0.150	0.067	42
35	0.113	0.020	0.180	0.068	78
Calculated	0.137	0.019	0.164	0.074	111

The average f values were 690, 910, and 1050 rps at 25, 30, and 35°C, respectively. The highest f was 1660 rps at 35°C. The average v values were 77, 100, and 116 μm/s at 25, 30, and 35°C. The highest v was 147 μm/s at 35°C. It should be noted that the cell with the fastest rotating flagellum was not the fastest swimming cell.

At each temperature, v had a tendency to saturate at high f. To show the feature more clearly, only the data at 35°C were replotted in Fig. 3 *b*. With increasing f, v tended to increase in the range below 1000 rps, while v remained rather constant above 1000 rps. This apparent saturation in v at high f was not observed or expected previously.

ANALYSIS WITH A MODEL

Model to analyze bacterial motion

We propose a hydrodynamic model to analyze the experimental results mentioned above. The schematic drawing of the model is shown in Fig. 4. In the model, the Stokes approximation was adopted and only a steady state was considered. Hydrodynamic interactions among a cell body, a flagellum, a glass surface, and other cells were neglected. The novel point of the model is that the torque characteristic of flagellar motor was taken into consideration. In hydrodynamic models proposed previously (Holwill and Burge, 1963; Chwang and Wu, 1971; Azuma, 1992; Ramia et al. 1993), the motor torque was eliminated as an unknown factor; consequently, only the ratio of v to f could be

TABLE 2 Parameters of cell and flagellum of a *Vibrio alginolyticus* YM42

Symbol	Parameter	Average (μm)	SD (μm)
$2a$	Cell width	0.80	0.09
$2b$	Cell length*	1.92	0.46
$2d$	Diameter of flagellar filament	0.032	0.004
L	Length of flagellar filament*	5.02	1.15
p	Pitch of flagellar helix	1.58	0.14
l	Filament length per pitch‡	1.82	0.16
r	Radius of flagellar helix	0.14	0.02

The parameters for 111 cells were determined by TEM.
*The difference between the average cell lengths obtained before and after LDM measurements was one-third of the standard deviation, whereas that for filament lengths was one-fourth of the standard deviation.
‡The pitch was also measured with an optical dark-field microscope, and the value was 1.5 ± 0.2 μm.

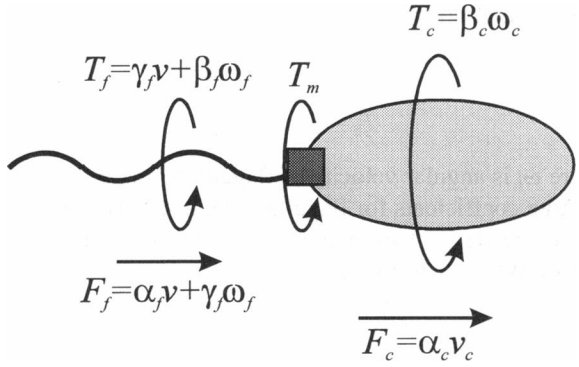

FIGURE 4 Schematic drawing of the model to analyze the bacterial swimming. F_c and F_f are drag forces from fluid to cell body and flagellum, T_c and T_f are drag torque to cell body and flagellum, T_m is torque generated by flagellar motor, v is swimming speed, ω_c and ω_f are angular velocities of cell body and flagellum, and α_c, β_c, α_f, β_f, and γ_f are drag coefficients.

discussed. As shown below, the present model can discuss not only the *v-f* ratio but also the apparent saturation shown in Fig. 3.

The equations of motion are

$$F_c + F_f = 0 \tag{3}$$

$$T_c - T_m = 0 \tag{4}$$

$$T_f + T_m = 0 \tag{5}$$

where F_c and F_f are drag forces from a fluid to a cell body and flagellum, T_c and T_f are drag torque to a cell body and flagellum, and T_m is torque generated by flagellar motor. Equation 3 is the equation of motion for the translational motion. Equations 4 and 5 are the equations of motion for the rotational motion of a cell body and flagellum, respectively.

The drag force and torque to a cell body can be written in the form of

$$F_c = \alpha_c v \tag{6}$$

$$T_c = \beta_c \omega_c \tag{7}$$

where v is swimming speed, ω_c is angular velocity of a cell body, and α_c and β_c are drag coefficients for a cell body. The cell body was assumed to be a spheroid, and the following drag coefficients α_c and β_c were adopted (Happel and Brenner, 1973):

$$\alpha_c = -6\pi\mu a\left\{1 - \frac{1}{5}\left(1 - \frac{b}{a}\right)\right\} \tag{8}$$

$$\beta_c = -8\pi\mu a^3\left\{1 - \frac{3}{5}\left(1 - \frac{b}{a}\right)\right\} \tag{9}$$

where μ is viscosity of medium and a and b are shorter and longer radii of spheroid.

The flagellar filament was assumed to be a rigid helix and to rotate on its helical axis. Then the drag force and torque

to the flagellum can be written in the form of

$$F_f = \alpha_f v + \gamma_f \omega_f \tag{10}$$

$$T_f = \beta_f \omega_f + \gamma_f v \tag{11}$$

where ω_f is angular velocity of flagellum, and α_f, β_f, and γ_f are drag coefficients for flagellum. Drag coefficients α_f, β_f, and γ_f are derived from Eqs. 6, 9, and 10 of Holwill and Burge (1963) as follows:

$$\alpha_f = -(8\pi^2 r^2 + p^2)C_0 \tag{12}$$

$$\beta_f = -(4\pi^2 r^2 + 2p^2)r^2 C_0 \tag{13}$$

$$\gamma_f = 2\pi r^2 p C_0 \tag{14}$$

$$C_0 = \frac{-2\pi\mu L}{(\log(d/2p) + 1/2)(4\pi^2 r^2 + p^2)} \tag{15}$$

where r and p are radius and pitch of flagellar helix, and d and L are radius and length of flagellar filament.

The following two types of motor torque, T_m, were assumed according to the experimental results (Manson et al., 1980; Lowe et al., 1987; Washizu et al., 1993; Iwazawa et al., 1993; Berg and Turner, 1993):

(Type 1) $$T_m = T_0 \tag{16}$$

(Type 2) $$T_m = T_0\left(1 - \frac{\omega_m}{\omega_0}\right), \quad \omega_m = \omega_f - \omega_c \tag{17}$$

where T_0 and ω_0 are constants, and ω_m is angular velocity of the motor. Type 1 of motor torque is constant independent of motor rotation rate, whereas type 2 of motor torque linearly decreases with increasing motor rotation rate.

Calculation of *v-f* ratio

From Eqs. 3, 6, and 10, the linear relation between v and f is obtained as follows:

$$v = -\frac{\gamma_f}{\alpha_c + \alpha_f}\omega_f. \tag{18}$$

The proportional coefficient $-\gamma_f/(\alpha_c + \alpha_f)$ (equal to *v-f* ratio if divided by 2π) does not change with temperature because the motor characteristics are not involved, and the viscosity is canceled (see Eqs. 8, 12, 14, and 15).

To calculate the value of the *v-f* ratio, cell and flagellar parameters measured by TEM (Table 2) were used. The standard deviations for the lengths of cell and flagellar filament were ~25%, whereas those for the other parameters were ~10%. In the calculation, therefore, the values of the lengths of cell and filament for individual cells were used, and the average values were used for the other parameters. It is noteworthy that no correlation between the lengths of cell and filament was observed (Fig. 5). Between "before" and "after" LDM measurements, no significant differences in the average cell and filament lengths were observed. The values of cell and filament lengths were not considered to change during the measurement.

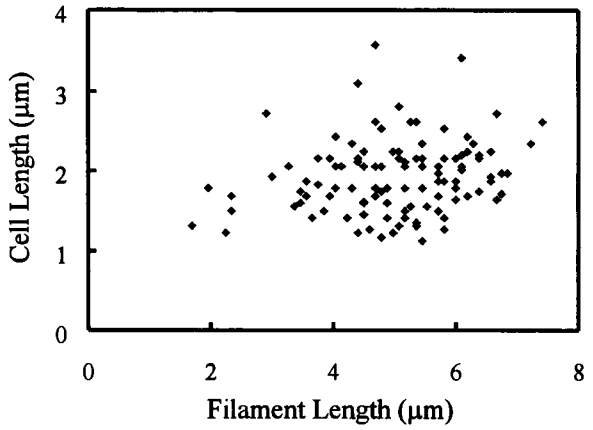

FIGURE 5 Relation between cell and filament lengths of *V. alginolyticus* YM42 measured by TEM. Each point represents data for an individual cell. The number of samples was 111.

The *v-f* ratios calculated for individual cells are summarized in Table 1. The average of the calculated *v-f* ratios was larger than that of the observed *v-f* ratios by ~20%. The standard deviation of the calculated *v-f* ratios agreed with that of the observed data. The distribution in the calculated *v-f* ratios was derived from the distribution of cell and filament lengths. Therefore, the wide distribution of experimental data points shown in Fig. 3 *a* is considered to originate from the distribution of cell and filament lengths.

Calculation of the relation between *v* and *f*

The roughly linear *v-f* relation could be explained by Eq. 18, which is essentially equivalent to the relation between v and f described in the previously proposed models (Holwill and Burge, 1963; Chwang and Wu, 1971; Azuma, 1992). The apparent saturation in v shown in Fig. 3 *b* could not be explained within the framework of the models. The equations of motion for rotation (Eqs. 4 and 5) and the motor-torque characteristic (Eq. 16 or 17) in addition to the equation of motion for translation (Eq. 3) were necessary to explain the whole feature observed in the experiment (Fig. 3).

The solutions can be analytically obtained for both type 1 and type 2 of torque characteristics (see Appendix). Both v and f can be calculated using the solutions if the values of viscosity, cell and flagellar parameters, and motor torque are given. In the calculation, the lengths of cell and filament for 50 individual cells that were randomly selected from the TEM data (Fig. 5) were used, and the average values were used for the other parameters (Table 2). For the viscosity of medium, the value of water was used (8.9, 8.0, and 7.3 millipoise at 25, 30, and 35°C). The values of motor torque used in the calculation were determined so as to fit the average of calculated f to that of the experiment. In type 1 of motor torque, T_0 were given to be 0.85, 1.01, and

1.06×10^{-18} N·m at 25, 30, and 35°C. In type 2, T_0 was assumed to be 1.5×10^{-18} N·m, and values of ω_0 were given to be 1700, 3000, and 3800 rps at 25, 30, and 35°C, respectively. Here we assumed that ω_0 depended on temperature, whereas T_0 did not, according to Iwazawa et al. (1993).

Fig. 6 shows the calculated f and v. The distributions of the calculated points for both type 1 and type 2 (Fig. 6, *a* and *b*) were similar to the experimental result (Fig. 3), although several points were distributed above 2000 rps in type 1. In both types, f and v tended to increase with increasing temperature. At each temperature, apparent saturation in v at high f was seen.

Solid lines in Fig. 6 show the v-f relations calculated using the assumed values of motor torque at 30°C when filament length was varied from 1.5–8.5 μm. The slowest and the fastest rotations on the line corresponded to the filament lengths of 8.5 and 1.5 μm, respectively; i.e., faster flagellar rotation associated with shorter flagellum. With decreasing filament length from 8.5 μm, f increased continuously. On the other hand, v increased first, and then tended to saturate in type 1 or to gradually decline in type 2. The data points were distributed around the calculated line. The deviation from the line was derived from the difference in cell length among cells.

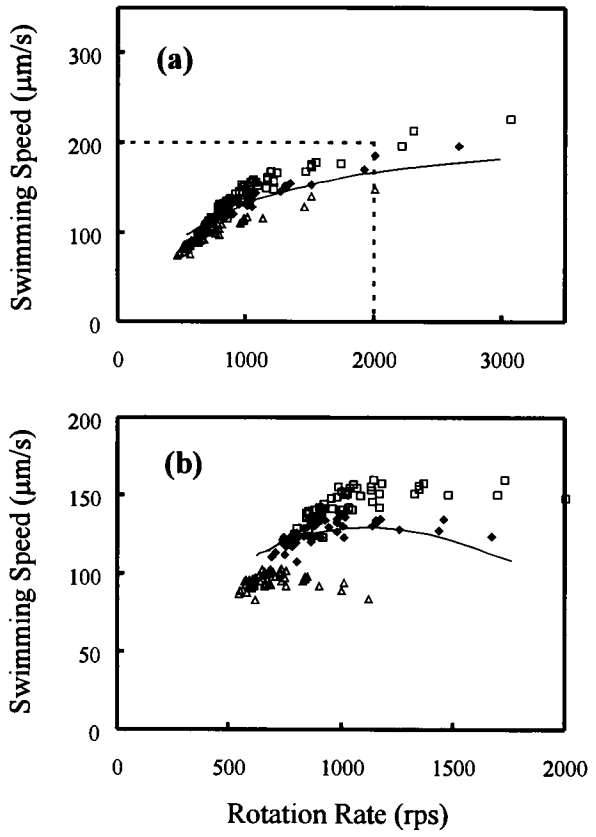

FIGURE 6 Calculated relation between flagellar rotation rate and swimming speed. Each point represents data calculated using cell and filament lengths selected randomly from Fig. 5 (*triangle*, 25°C; *diamond*, 30°C; *square*, 35°C). The solid lines represent the relation between f and v calculated using assumed values of motor torque at 30°C when filament length was varied from 1.5 μm (the fastest rotation) to 8.5 μm (the slowest rotation). (*a*) Type 1 of torque characteristic (constant torque independent of rotation rate) was used in the calculation. To represent all points, the range of axes is expanded. The frame indicated by dashed lines shows the same area as in Figs. 3 and 6 *b*. (*b*) Type 2 of torque characteristic (linearly decreasing torque with rotation rate) was used in the calculation.

DISCUSSION

LDM has been used to observe the fast rotation of single flagella on cells stuck to a glass slide (Kudo et al., 1990). In this study, we successfully obtained a wide range of v and f of individual free-swimming cells by using LDM. We used the *V. alginolyticus* mutant YM42, which swam smoothly and had only a single polar flagellum (no lateral flagella). This simplified the analysis of the v-f data.

The v-f data exhibited roughly linear relation. The average v-f ratios at different temperatures were almost the same, and the values indicated that *V. alginolyticus* cells progressed by 7% of the pitch of flagellar helix per flagellar rotation. Apparent saturation in v at high f was observed at each temperature. The highest rotation rate observed in the experiment was 1660 rps. As previously reported (Magariyama et al., 1994), the value was much larger than those reported previously of 100 rps for *Streptococcus* at 22°C (Lowe et al., 1987), 270 rps for *E. coli* at 32°C (Lowe et al., 1987), and 170 rps for *S. typhimurium* at 30°C (Kudo et al., 1990).

We proposed a new model to analyze the experimental results obtained in the present study. Previous models (Holwill and Burge, 1963; Chwang and Wu, 1971; Azuma, 1992; Ramia et al. 1993) could discuss only the v-f ratios. Consequently, they could not discuss changes in v and f according to flagellar length differences among cells, hence apparent saturation (Fig. 3). To evaluate such effects, the torque characteristic of flagellar motor was considered in the present model. The model was simple enough to be analytically solved and could qualitatively explain the experimental results, including the apparent saturation that had not been predicted in previous work.

Discrepancy between the experimental and the calculated results

Although the model qualitatively explained the experimental results, there was some quantitative discrepancy between the experimental and the calculated results. For example, the average of the experimentally obtained v-f ratios was 20% smaller than the calculated one. The oversimplification in the model may cause such discrepancy. We ignored several factors such as deformation of flagellum during rotation, hydrodynamic wall effect, hydrodynamic interaction between cell body and flagellum, and displacement of the longer axis of the cell off the flagellar axis.

The first factor changes the *v-f* ratio. For example, if the length of flagellar helix decreases by 5% without winding or unwinding, the *v-f* ratio is estimated to increase by 21%. The second factor is considered to increase the *v-f* ratio. Almost all bacteria were observed to swim near and parallel to the glass slide, so they should experience hydrodynamic wall effect. Ramia et al. (1993) showed that such effect would increase the mean swimming speed by less than 10%. The third factor is considered to decrease the *v-f* ratio. Higdon (1979) pointed out that hydrodynamic interaction between cell body and flagellum should decrease swimming speed by ~20%.

The fourth factor is also considered to decrease the *v-f* ratio. The flagellar axis is actually displaced from the longer axis of the cell because the rod of the motor is connected to the flagellar filament and not to the axis of the flagellar helix. Therefore, swing of the cell body should occur. We actually observed the maximum cell swing of 30°, which was estimated to decrease swimming speed by 3%. The fourth factor should also cause bending of the flagellar helix, as indicated before (Fig. 2 *b*). The helix bending should decrease the effective length of flagellar screw and hence the swimming speed.

The total effect of the above factors might cause the discrepancy between the experimental and the calculated results.

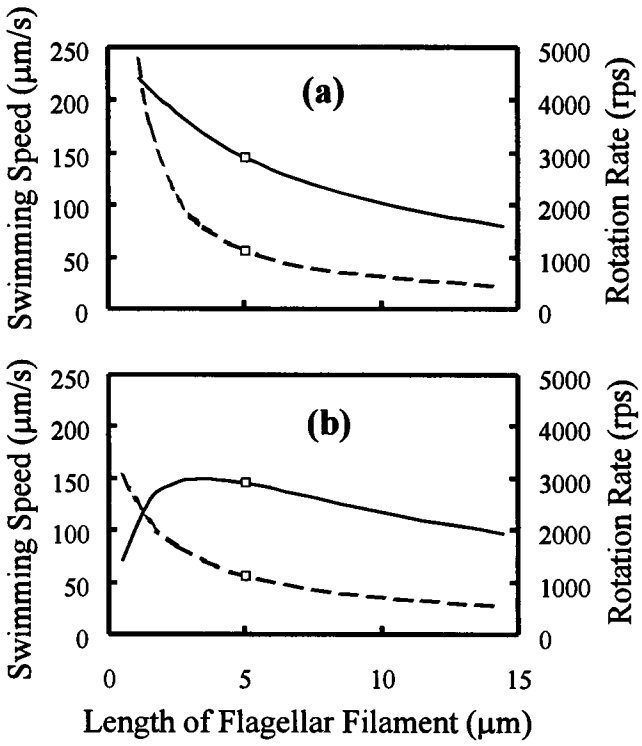

FIGURE 7 Calculated swimming speed and motor rotation rate as functions of filament length. The values of motor torque at 35°C (assumed in the text) were used in the calculation. Solid and dashed lines represent swimming speed and motor rotation rate, respectively. Square symbols indicate the values calculated using the average filament length measured by TEM. (*a*) Type 1 of torque characteristic was used. (*b*) Type 2 of torque characteristic was used.

Torque characteristic of the flagellar motor

The dependence of motor torque on rotation rate is an important characteristic used to study the energy transduction mechanism of the flagellar motor. In the model, we assumed two types of torque characteristics, that is, constant torque independent of motor rotation rate (type 1) and linearly decreasing torque with increasing motor rotation rate (type 2). Type 1 of torque characteristic was reported by Manson et al. (1980) and Washizu et al. (1993), and type 2 was reported by Lowe et al. (1987) and Iwazawa et al. (1993). Berg and Turner (1993) reported that the torque characteristic was type 1 in the range of slow rotation and type 2 in the range of fast rotation (corresponding to the range of free swimming).

The calculated *v-f* data for type 1 were distributed more widely than the experimental result (Figs. 3 *a* and 6 *a*), whereas those for type 2 were distributed within almost the same range as the experimental result (Figs. 3 *a* and 6 *b*). To further investigate the feature, calculated motor rotation rate and *v* as functions of filament length are shown in Fig. 7. For type 1, the rotation rate infinitely increased with decreasing filament length. Although the rotation rate increased steeply, *v* increased only gradually because efficiency of propulsion diminished with decreasing filament length (see the next section). For type 2, the rotation rate increased to a finite value (ω_0), and *v* decreased to zero as filament length approached zero. Thus differences between the two types were obvious in the range of shortest filament length. LDM data for cells having flagella shorter than ~4 μm, however, might not be obtained in the present study because LDM signals from very short flagella were merged into stronger signals from cell bodies. If *f* of shortest flagella could be measured, torque characteristic of flagellar motor would be evaluated from the experimental *v-f* relation.

Motor torque was estimated for the polar flagellum of *V. alginolyticus* so as to fit the calculated *f* to that of the experiment (Fig. 6). For example, at 25°C, T_0 (torque at zero rotation rate) was estimated to be $\sim 1\times10^{-18}$ N·m (in both type 1 and type 2). Values of T_0 reported for other species were 2.5×10^{-18} N·m for *Streptococcus* at 22°C (Lowe et al., 1987) and 6.5×10^{-18} N·m for *E. coli* at 23.5°C (Iwazawa et al., 1993). These values indicate that the polar flagellar motor of *V. alginolyticus* can generate torque a little smaller than others. On the other hand, the rotation rate of *V. alginolyticus* polar flagellum was much higher than those of others, as mentioned above. The polar flagellar motor of *V. alginolyticus* seems to be optimized to rotate fast in the low viscosity medium where large torque is not necessary. *V. alginolyticus* is known to use lateral flagella instead of a polar flagellum under high viscosity condition (Baumann and Schubert, 1984). Thus accurate torque characteristics of both motors are desired to be determined.

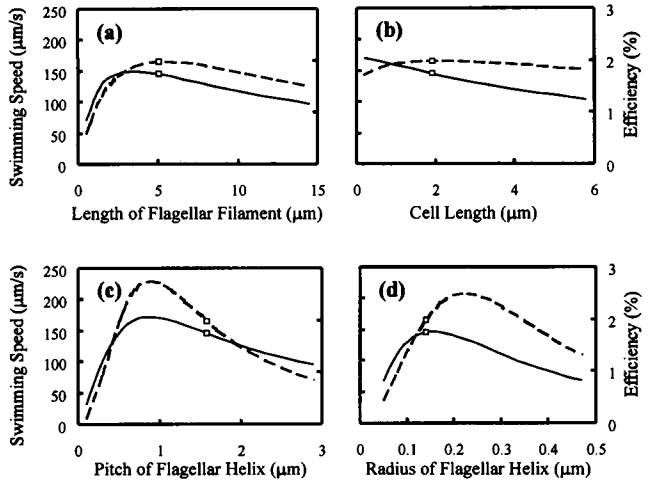

FIGURE 8 Calculated swimming speeds and efficiencies of cell propulsion as functions of filament length (*a*), cell length (*b*), pitch of flagellar helix (*c*), and radius of flagellar helix (*d*). Type 2 of torque characteristic was adopted, and the assumed values of motor torque at 35°C were used in the calculation. Solid and dashed lines represent swimming speed and efficiency, respectively. Square symbols indicate the values calculated using the average values of respective parameters measured by TEM.

The motor torque for an individual cell would be calculated from the *v-f* data if the parameters of cell and flagellum for the cell were determined. Among the parameters, cell and filament lengths might be determined from the temporal lengths of CELL and FLA parts of LDM data (Fig. 2). However, the temporal length of the CELL part increased two to three times because of the high intensity of the scattered light from the cell body. This caused large error values in determining both cell and filament lengths. Therefore we did not use the cell and filament lengths determined by LDM data in the analysis.

At each temperature, the experimentally obtained v values at any f were distributed more widely than were the calculated v values. This suggests that some parameters that were not considered in the model affected the distribution. The difference in torque among flagellar motors may be one of such parameters. If the motor torque becomes larger, the data points shift toward the upper right direction in Fig. 6, and vice versa. Thus the wide distribution of *v-f* at each temperature might be caused by the difference of motor torque characteristic among cells.

Effect of bacterial shape on v and η

On the basis of the model, we examined the effect of cell and flagellar parameters of a *V. alginolyticus* cell on swimming speed and efficiency of cell propulsion. We define the efficiency, η, as the ratio of the work per unit time for cell propulsion to the power of flagellar motor,

$$\eta = \frac{F_c v}{T_m \omega_m}. \tag{19}$$

It should be noted that η is independent of motor torque (see Appendix).

Fig. 8 shows v and η calculated using type 2 of torque characteristic as functions of filament length, cell length, pitch of flagellar helix, and radius of flagellar helix. The maximums of calculated η were near the average lengths of filament and cell measured by TEM (Fig. 8, *a* and *b*) but far from the average pitch and radius of flagellar helix (Fig. 8, *c* and *d*). It is noteworthy that η decreased only slightly in the actual range of filament and cell lengths (2–8 μm and 1–2 μm, respectively). The maximum of calculated v values deviated from the average values of the parameters except for radius of helix.

The results showed that the lengths of cell and filament, which change with growth, are considered to be almost optimized for η. On the other hand, pitch and radius of flagellar helix, which have genetically fixed values, seem not to be optimized for η. Therefore, the results suggest that the evolution of the flagellar shape of bacteria has not necessarily been optimized for swimming.

We thank F. Oosawa, M. Esashi, and H. Miura for support and discussions; S. Asakura, S. Tsuge, H. Yoshimura, Y. Mikuriya, and M. Homma for discussions; and H. C. Berg for critical reading of the manuscript.

APPENDIX

The solutions of the simultaneous equations (Eqs. 3, 4, 5, 6, 7, 10, 11, and 16 or 17) are summarized as follows:

$$v = K_0 \beta_c \gamma_f \tag{20}$$

$$\omega_c = K_0(\alpha_c \beta_f + \alpha_f \beta_f - \gamma_f^2) \tag{21}$$

$$\omega_f = -K_0(\alpha_c \beta_c + \alpha_f \beta_c) \tag{22}$$

$$\omega_m = -K_0(\alpha_c \beta_c + \alpha_c \beta_f + \alpha_f \beta_c + \alpha_f \beta_f - \gamma_f^2) \tag{23}$$

$$F_c = -F_f = -K_0 \alpha_c \beta_c \gamma_f \tag{24}$$

$$T_c = -T_f = T_m = K_0(\alpha_c \beta_c \beta_f + \alpha_f \beta_c \beta_f - \beta_c \gamma_f^2). \tag{25}$$

For type 1 of torque characteristic (Eq. 16),

$$\frac{1}{K_0} = \frac{\alpha_c \beta_c \beta_f + \alpha_f \beta_c \beta_f - \beta_c \gamma_f^2}{T_0}. \tag{26}$$

For type 2 of torque characteristic (Eq. 17),

$$\frac{1}{K_0} = \frac{\alpha_c \beta_c \beta_f + \alpha_f \beta_c \beta_f - \beta_c \gamma_f^2}{T_0} - \frac{\alpha_c \beta_c + \alpha_c \beta_f + \alpha_f \beta_c + \alpha_f \beta_f - \gamma_f^2}{\omega_0}. \tag{27}$$

Using the above solutions, the efficiency of cell propulsion η (Eq. 19) is rewritten regardless of the type of torque characteristics as follows:

$$\eta = \frac{\alpha_c \beta_c \gamma_c \gamma_f}{(\alpha_c \beta_c + \alpha_c \beta_f + \alpha_f \beta_c + \alpha_f \beta_f - \gamma_f^2)(\alpha_c \beta_f + \alpha_f \beta_f - \gamma_f^2)}. \tag{28}$$

REFERENCES

Azuma, A. 1992. The Biokinetics of Flying and Swimming. Springer-Verlag, Tokyo.

Baumann, P., and R. H. W. Schubert. 1984. Vibrio. *In* Bergey's Manual of Systematic Microbiology, Vol. 1. N. R. Krieg, et al., editors. Williams & Wilkins, Baltimore. 518–538.

Berg, H. C., and S. Khan. 1982. A model for the flagellar rotary motor. *In* Mobility and Recognition in Cell Biology. H. Sund and C. Veeger, editors. deGruyter, Berlin. 485–497.

Berg, H. C., and L. Turner. 1993. Torque generated by the flagellar motor of *Escherichia coli. Biophys. J.* 65:2201–2216.

Blair, D. F., and H. C. Berg. 1990. The MotA protein of *E. coli* is a proton-conducting component of the flagellar motor. *Cell.* 60:439–449.

Chwang, A. T., and T. Y. Wu. 1971. A note on the helical movement of micro-organisms. *Proc. R. Soc. Lond. B.* 178:327–346.

Gibbons, I. R. 1981. Cilia and flagella of eukaryotes. *J. Cell Biol.* 91: 107s–124s.

Francis, N. R., G. E. Sosinsky, D. Thomas, and D. J. DeRosier. 1994. Isolation, characterization, and structure of bacterial flagellar motors containing the switch complex. *J. Mol. Biol.* 235:1261–1270.

Happel, J., and H. Brenner. 1973. Low Reynolds Number Hydrodynamics. Kluwer Academic Publishers, Dordrecht.

Higdon, J. J. L. 1979. The hydrodynamic of flagellar propulsion: helical waves. *J. Fluid Mech.* 94:331–351.

Hirota, N., and Y. Imae. 1983. Na^+-driven flagellar motors of an alkalophilic *Bacillus* strain YN-1. *J. Biol. Chem.* 258:10577–10581.

Holwill, M. E. J., and R. E. Burge. 1963. A hydrodynamic study of the motility of flagellated bacteria. *Arch. Biochem. Biophys.* 101:249–260.

Iwazawa, J., Y. Imae, and S. Kobayashi. 1993. Study of the torque of the bacterial flagellar motor using a rotating electric field. *Biophys. J.* 64:925–933.

Kudo, S., Y. Magariyama, and S.-I. Aizawa. 1990. Abrupt changes in flagellar rotation observed by laser dark-field microscopy. *Nature.* 346: 677–680.

Lauger, P. 1988. Torque and rotation rate of the flagellar motor. *Biophys. J.* 53:53–66.

Lowe, G., M. Meister, and H. C. Berg. 1987. Rapid rotation of flagellar bundles in swimming bacteria. *Nature.* 325:637–640.

Macnab, R. M. 1987. Motility and chemotaxis. *In Escherichia coli* and *Salmonella typhimurium.* F. C. Neidhardt et al., editors. American Society of Microbiology, Washington, DC. 732–759.

Magariyama, Y., S. Sugiyama, K. Muramoto, Y. Maekawa, I. Kawagishi, Y. Imae, and S. Kudo. 1994. Very fast flagellar rotation. *Nature.* 371:752.

Manson, M. D., P. M. Tedesco, H. C. Berg, F. M. Harold, and C. van der Drift. 1977. A protonmotive force drives bacterial flagella. *Proc. Natl. Acad. Sci. USA.* 74:3060–3064.

Manson, M. D., P. M. Tedesco, and H. C. Berg. 1980. Energetics of flagellar rotation in bacteria. *J. Mol. Biol.* 138:541–561.

Matsuura, S., J. Shioi, and Y. Imae. 1977. Motility in *Bacillus subtilis* driven by an artificial protonmotive force. *FEBS Lett.* 82:187–190.

Oosawa, F., and S. Hayashi. 1983. Coupling between flagellar motor rotation and proton flux in bacteria. *J. Physiol. Soc. Jpn.* 52:4019–4028.

Oosawa, K., T. Ueno, and S.-I. Aizawa. 1994. Overproduction of the bacterial flagellar switch proteins and their interactions with the MS ring complex *in vitro. J. Bacteriol.* 176:3683–3691.

Ramia, M., D. L. Tullock, and N. Phan-Thien. 1993. The role of hydrodynamic interaction in the locomotion of microorganisms. *Biophys. J.* 65:755–778.

Shimada, K., T. Ikkai, T. Yoshida, and S. Asakura. 1976. Cinematographic analysis of the movement of flagellated bacteria. II. The ratio of the propulsive velocity to the frequency of the wave propagation along flagellar tail. *J. Mechanochem. Cell Motil.* 3:185–193.

Schuster, S. C., and S. Khan. 1994. The bacterial flagellar motor. *Annu. Rev. Biophys. Biomol. Struct.* 23:509–539.

Silverman, M., and M. Simon. 1974. Flagellar rotation and mechanism of bacterial motility. *Nature.* 249:73–74.

Yamaguchi, S., S.-I. Aizawa, M. Kihara, M. Isomura, C. J. Jones, and R. M. Macnab. 1986. Genetic evidence for a switching and energy-transducing complex in the flagellar motor of *Salmonella typhimurium. J. Bacteriol.* 168:1172–1179.

Washizu, M., Y. Kurahashi, H. Iochi, O. Kurosawa, S.-I. Aizawa, S. Kudo, Y. Magariyama, and H. Hotani. 1993. Dielectrophoretic measurement of bacterial motor characteristics. *IEEE Trans. Ind. Appl.* 29:286–294.